MAGIC-TDAS 06-09
060719 / E. Oña-Wilhelmi
20 July 2006

Observations under moonlight and twilight with MAGIC

E. Oña-Wilhelmi, J. Rico, J. Cortina, N. Sidro and R. Firpo

Institut de Física d'Altes Energies (IFAE)
Edifici Cn. Universitat Autònoma de Barcelona
08193 Bellaterra (Barcelona) Spain

One small step for man, one giant leap for mankind

Neil Amstrong

Abstract

One of the unique features of MAGIC is its capability to observe under moderate moonlight. This allows to increase the duty cycle by a ∼50% and a better sampling of variable sources is possible. In this paper we present a study of the effect of the moonlight on the telescope's performance. In order to understand this effect, we have analyzed Crab Nebula data recorded by MAGIC during periods when the moon was shining and compared the results with standard (dark) Crab Nebula observations in terms of efficiency and sensitivity. We also study the energy dependence of these effects, compare the results with Monte Carlo (MC) simulations and propose the best strategy for moon observations and data analysis.

1 Introduction

MAGIC has an average duty cycle per year of about 11% under strict condition of dark observations, i.e. between astronomical dusk and dawn and with the moon below the horizon. If this requirement is relaxed to allow observations under moderate moonlight or twilight, an increase of the duty cycle to 17% (from ∼1000 to ∼1500 hours of observations per year) is possible. Moon datataking in addition allows a more uniform coverage of variable sources, preventing biases in periodicity analyses.

Traditionally, the photo-multiplier tubes (PMTs) of Cherenkov telescopes are operated under amplification gains up to 10^8 which, under moonlight, generate currents that can damage the last dynodes. HEGRA CT1 telescope pioneered the regular operations under moderate moonlight [1], lowering the PMT high voltages (HV). Previous works by [2] and [3] successfully proved the possibility of observing during moonshine. They both used PMTs sensible to the UV range, either solar blind photomultipliers, or wavelength shifters. MAGIC camera was designed to operate under increased light background, with no need to lower the HVs. It is equipped with PMTs that run at a gain of less than 10^5 [4], avoiding high currents in the PMT last dynodes. For dark observations the anode current is about 1μA and increases by as much as a factor 30-50 with full moon. This increase depends on factors such as the telescope and moon zenith angle, angular distance between the telescope and the moon and the atmospheric conditions. In order to avoid the PMT cathode degradation, the maximum allowed mean DC is 7μA, with a maximum individual value of 20μA. These limits allow the observation in the presence of the moon until (since) 4 days before (after) full moon, for certain positions of the moon in the sky and angular distances between the moon and the observed source [4].

The increase in the light of night sky (LONS) produced by the moon enhances the probability of accidental triggers. Therefore, the trigger discriminator threshold (DT) must be increased accordingly, thus ensuring a low rate of accidentals and keeping the total rate below the data acquisition system (DAQ) technical maximum rate ($\sim$500 Hz). An increase of the DTs can affect the image parameters, so in order to study its impact on gamma ray efficiency and source detection sensitivity we have analyzed a sample of Crab Nebula observations under different moonlight conditions. We have compared our results with MC simulations. After a description of the data sample and data reduction chain in Section 2, we will present a description of the effects of the moon on the reconstruction of the shower images, based on real data (Section 3) and MC simulated gamma events (Section 4). In Section 5 we present the results on the gamma efficiency and sensitivity. Next, we study the energy dependence of such effects (Section 6), including a study of the energy/size threshold evolution. Finally, we draw some conclusions and give some recommendations for moonlight data acquisition and analysis.

2 Data Sample and Analysis Procedure

In the following analysis, we have used data from Crab Nebula observations at different light conditions, performed between January –right after a redefinition of DT default values– and March 2006. This includes dark observations, used as a reference. Table 1 summarizes the different samples that will be used throughout the paper. The data were classified into two groups according to the zenith angle, namely below 30° and between 30° and 40°. Both groups are studied separately and later the results are merged. A special test was performed on 2006/03/05 using high DT values during a dark observation.

During the analyzed periods, the default value of the DT when observing a galactic source such as the Crab Nebula is 35 (arbitrary units), and the mean DC of about 1.0 μA. Under moonlight, DC increases. The initial DTs are set to a fixed value considering the mean DC and other factors, such as the moon phase, the distance moon-source, and the moon zenith angle [4]. Since only the so-called inner camera plays a role in the trigger discrimination, DTs are only set within this area. The mean DC and DT shown in Table 1 are averaged both, for all the pixel in the inner camera and for the total observation time. In the graphs that will be presented in the following sections, each point corresponds to a particular observation day, further subdivided into finer DC and/or DT bins whenever possible. The samples at zenith angle between 20° and 30° for the days 2006/01/22, 2006/02/04, 2006/02/05 correspond to three different light conditions, namely dark, moderate and strong moonlight, respectively, and are used in the next sections to illustrate the effect of moonlight.

Date	T[min]	θ[deg]	Moon Conditions	<DC> [μA]	<DT>
2006/01/22	**34**	**8-14**	**Dark**	**1.0**	**35**
2006/02/03	57	8-20	Moon	1.5	40
2006/02/04	**107**	**8-28**	**Moon**	**2.4**	**47**
2006/02/05	**82**	**9-29**	**Moon**	**4.5**	**60**
2006/02/18	15	27-30	Moon	1.8	60
2006/02/20	22	24-30	Dark	1.2	35
2006/02/21	52	7-19	Dark	1.2	35
2006/02/22	94	7-19	Dark	1.2	38
2006/03/04	25	24-30	Moon	1.5	45
2006/02/05	7	30-40	Moon	4.2	61
2006/02/20	44	30-40	Dark	1.2	35
2006/02/24	30	33-40	Dark	1.2	35
2006/03/04	42	30-40	Moon	1.5	46
2006/03/05	42	32-40	Moon	2.6	50
2006/03/06	46	32-40	Moon	5.2	66
2006/03/23	32	30-38	Dark	1.2	35
2006/03/25	34	31-38	Dark	1.2	38
2006/03/29	20	35-39	Dark	1.3	36
2006/03/05	**35**	**48-54**	**Dark**	**1.1**	**55**
Total	12.3 h	8-40	–	1.0 - 5.2	35-66

Table 1: Crab Nebula data sets used in the present analysis. From left to right: observation date (corresponding to the date after midnight of the observation night), observation time, zenith angle, light conditions, mean DC and mean DT (measured in arbitrary units). All available runs from the specified dates and zenith angle intervals are used. The highlighted entries correspond to the samples that are used as example to illustrate the different effects. Separated by horizontal lines, from top to bottom: observations at zenith angle between 20° and 30°, observations at zenith angle between 30° and 40° and special test.

The data were processed by the on-site analysis running at La Palma (Mars version 0.10.3 [5], signal extracted with the Digital Filter [6], calibration using the excess noise factor method [7], absolute image cleaning with levels 10 and 5 phe for core and boundary pixels, respectively). Quality cuts based on the trigger rate and after cleaning rates are applied in order to remove bad weather runs and runs containing accidental triggers produced by cars or satellites. Spark events are removed using a standard cut on the $\log_{10}$(SIZE)-$\log_{10}$(CONC) plane. Gamma/hadron separation is performed using the Random Forest classification method, trained with MC simulated gamma-ray events and data from galactic empty fields of view. An independent random forest was grown for each of the two zenith angle samples. In all cases, the MC and data samples which were used to train the forests correspond to dark observations. The signal region is defined by the cuts HADRONNESS$<$0.15 and ALPHA$<8^\circ$ (non-optimized).

Several dedicated samples of MC gamma-ray events were used to compare with the results obtained with Crab Nebula data. The MC standard production [8] up to reflector files (CORSIKA v6.0.19, reflector v6.0) was used as a starting point. The LONS level and/or the DT were then increased in the input data card of the camera program (camera CVS version as of February 11th, 2006). MC files were processed in the same way as real data. Table 2 summarizes the different MC sets.

Set	θ [deg]	LONS level	DT (mV)
1	0-30	$LONS_0$	4
		$2\times LONS_0$	4
		$4\times LONS_0$	4
		$4\times LONS_0$	6
		$4\times LONS_0$	8
		$4\times LONS_0$	10
2	20-30	$4\times LONS_0$	4
		$4\times LONS_0$	10
		$4\times LONS_0$	30
		$4\times LONS_0$	50
3	20-30	$LONS_0$	4
		$LONS_0$	10
		$LONS_0$	30
		$LONS_0$	50
4	30-40	$LONS_0$	4

Table 2: Monte Carlo samples used in the present analysis. From left to right: set identifier (used as a reference throughout the paper), zenith angle, level of LONS (where $LONS_0$ is the default in the camera data card, i.e. 0.13 phe/ns 0.1×0.1 deg^2 239 m^2), and discriminator threshold level (4 mV is the standard value).

3 Effect of the Moonlight on Real Data

As explained above, when observing under moonlight, an increase of the rate of accidental events is avoided at hardware level by increasing the DT. Under such conditions, it is clear that showers with low light content (i.e. low SIZE) have a lower probability to trigger the telescope, and the distribution of SIZE is depleted at low values. However, we find that showers at SIZE values up to 10^4 phe, i.e. those well above the trigger level, are also suppressed. The effect is illustrated in Figure 1. The trigger and cleaning rates for the three samples are shown in Table 3. In order to understand the loss of events at high SIZE values, we have performed several checks, summarized below.

Date	Light	Trigger Rate [Hz]	Clean. Rate [Hz]
2006/01/22	Dark	260	115
2006/02/04	Moderate moonlight	200	85
2006/02/05	Strong moonlight	160	55

Table 3: Trigger and cleaning event rates for three Crab Nebula samples under different moonlight conditions (see Table 1 for details).

One might think that the increase of LONS results in a malfunction of the calibration software. We have compared the calibration constants in the different samples (see Figure 2). We find no significant effect.

Next, we have compared the distributions of the Hillas variables. This is not only relevant to understand the loss of showers with large SIZE, but also to understand inefficiencies in the following steps of the analysis chain where cuts in these parameters are applied. Figures 3, 4 and 5 show, respectively, the LENGTH, WIDTH and CONC distributions for a variety of SIZE

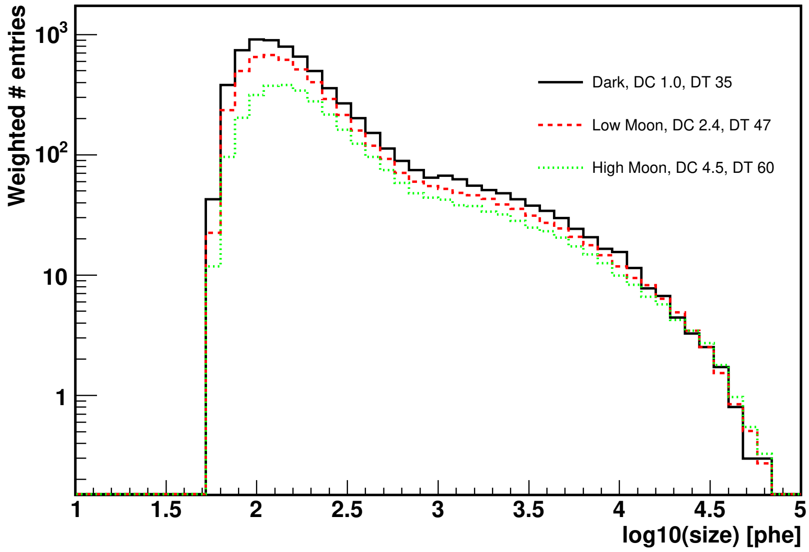

Figure 1: Distribution of SIZE for events after image cleaning, for three Crab Nebula samples: dark observation (black, solid line), observations under moderate moonlight (red, dashed line) and under strong moonlight (green, dotted line). The curves are normalized to a common observation time.

lower cuts. There is no significant difference in the shape of the distributions for SIZE above 200 phe. Below this value the distributions are distorted by the different trigger threshold. A study of the effect of the moonlight on the threshold is presented in section 6. Since these parameters have the highest discrimination power between gamma and hadron events, we do not expect gamma/hadron separation to degrade due to the moon light.

The situation is somewhat different for the DIST distribution (Figure 6). In this case we find differences at all SIZE cut values. Figure 7 shows again the DIST distributions after normalization to a common observation time. The distributions for SIZE cuts 0 and 200 phe are dominated by showers which are close to the trigger level, therefore we lose events at all values of DIST. In contrast, for a SIZE cut of 400 phe and above the showers get lost only for large DIST ($\geq 0.8°$). This suggests that showers that are not fully contained in the trigger are more sensitive to the increase in DT. To further check this hypothesis we plot the DIST distribution for showers which are fully contained in the inner camera (which in approximation corresponds to the trigger region). If the loss of events is due to the increase of the DT values, we do not expect it to show up in this subsample. On the other hand, if the dominant cause of the loss is the increase of LONS, it will be also present in this subsample. The results are shown in Figure 8. For a SIZE cut of 400 phe (i.e. well above the trigger level) the distributions for the different moonlight conditions (corresponding to different DT values) agree. This confirms that the loss of showers at all SIZE values is related with the increase of the DT values.

To illustrate this effect, a schematic representation is drawn in Figure 9. Images with low SIZE (shower A and top-left distribution in Figure 7) have a lower probability of passing the trigger in presence of the moon, due to the increased DTs, independently of their DIST value. Indeed, for high enough DIST, such showers are not recorded simply because they lay out of the trigger area. Large showers (showers B and C, and bottom distributions in Figure 7) are in principle well above the trigger level. However, when DIST is large, an important fraction of the

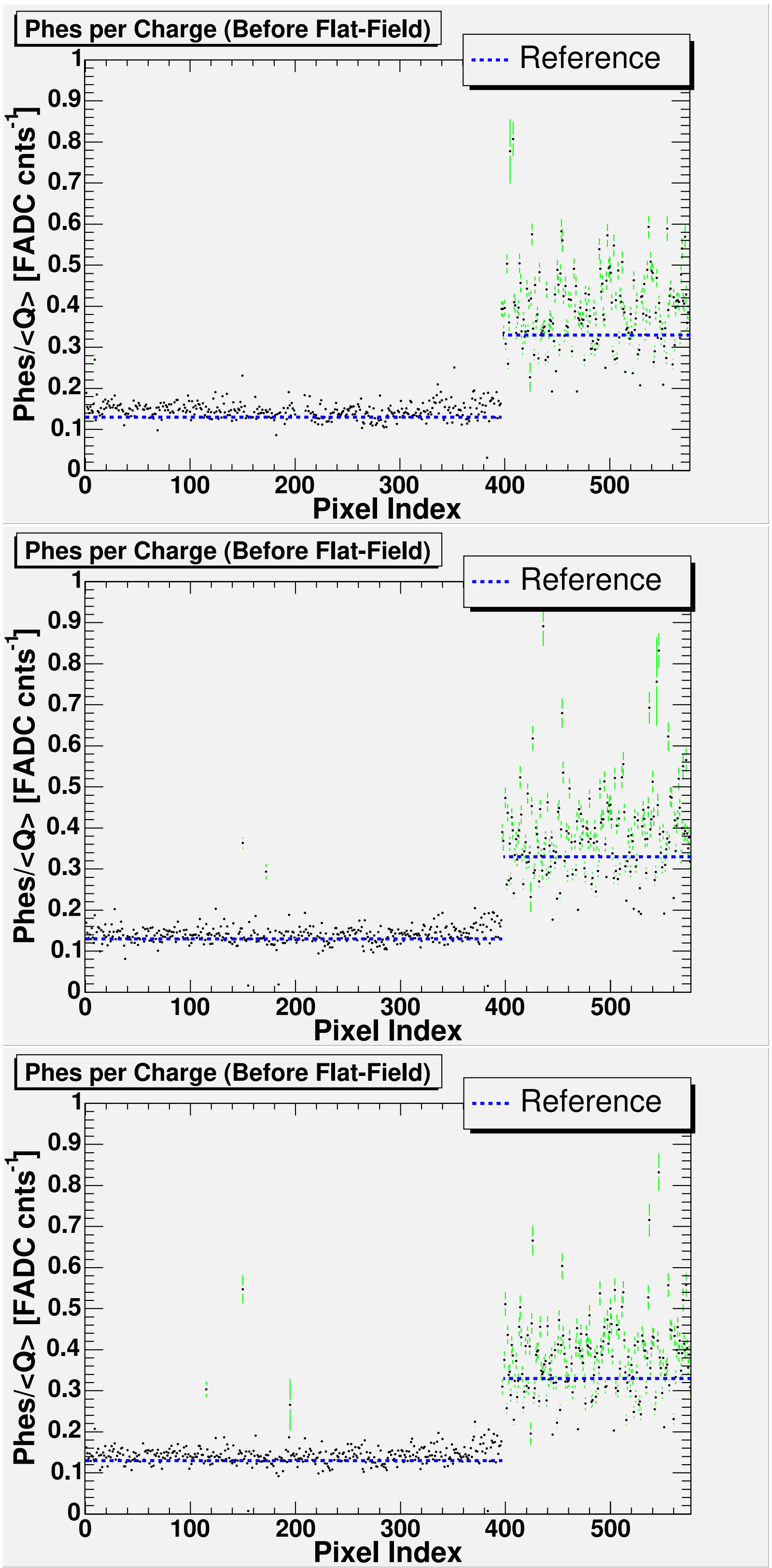

Figure 2: Conversion factors as a function of pixel index for three Crab Nebula samples taken under different moonlight conditions. From top to bottom: dark, moderate moonlight and strong moonlight observations.

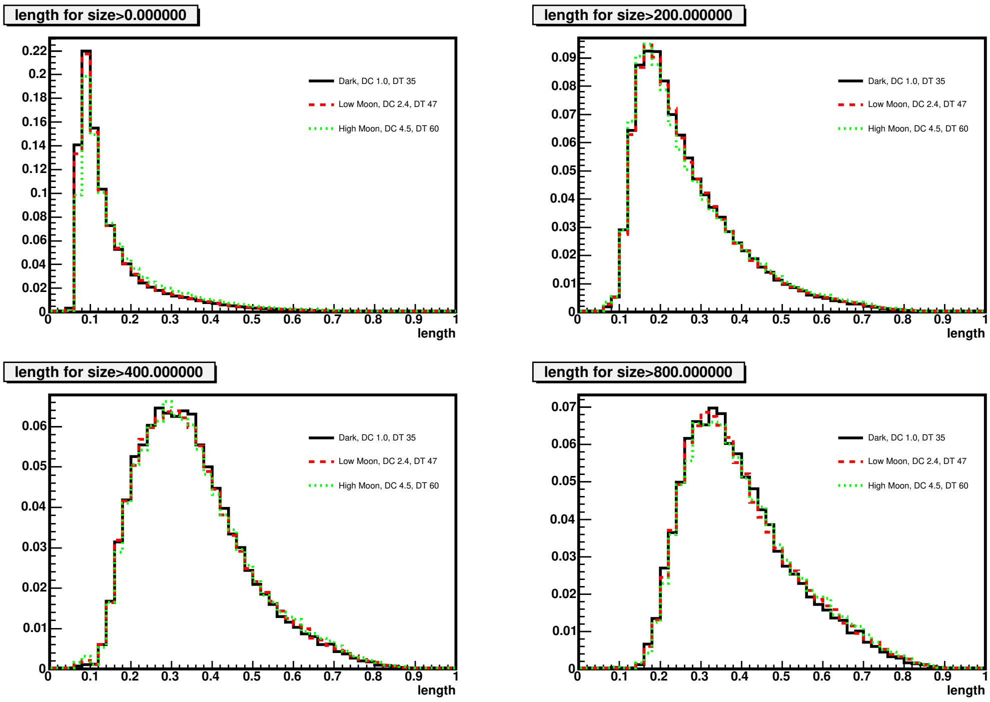

Figure 3: Distributions of LENGTH (in degrees) for three Crab Nebula samples with different moonlight conditions and different SIZE lower cuts. The histograms are normalized to unit area.

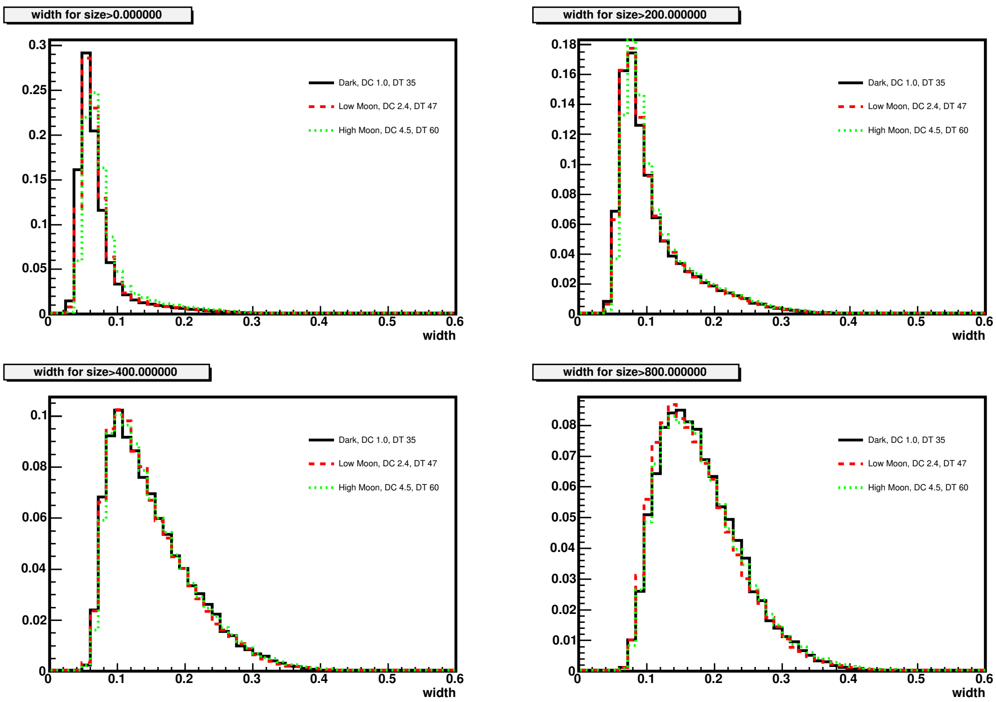

Figure 4: Distributions of WIDTH (in degrees) for three Crab Nebula samples with different moonlight conditions and different SIZE lower cuts. The histograms are normalized to unit area.

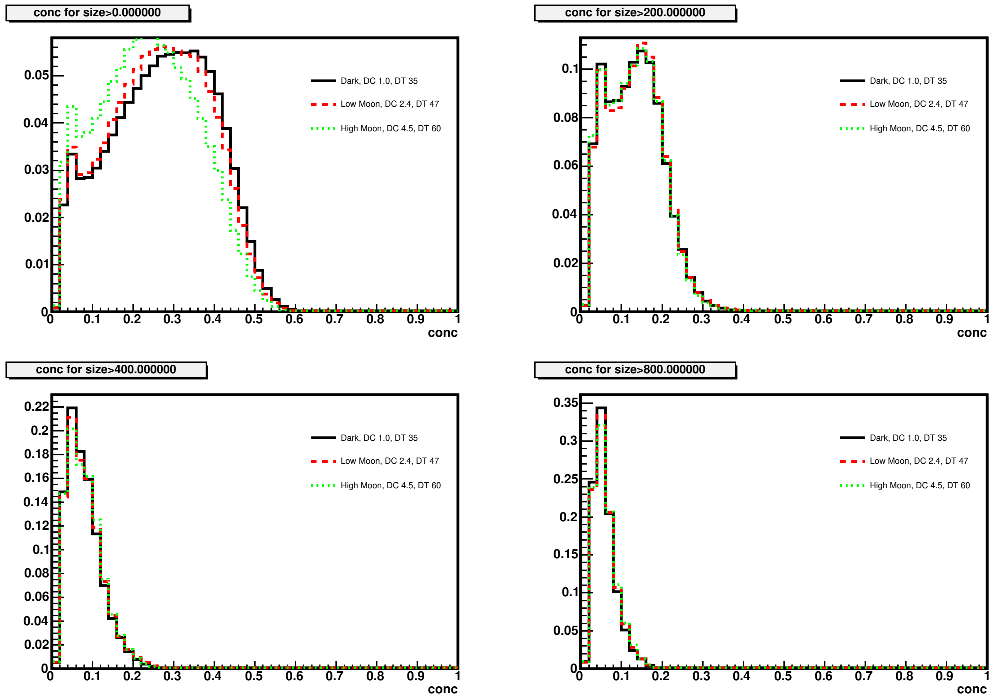

Figure 5: Distributions of CONC for three example Crab Nebula samples with different moonlight conditions and different SIZE lower cuts. The histograms are normalized to unit area.

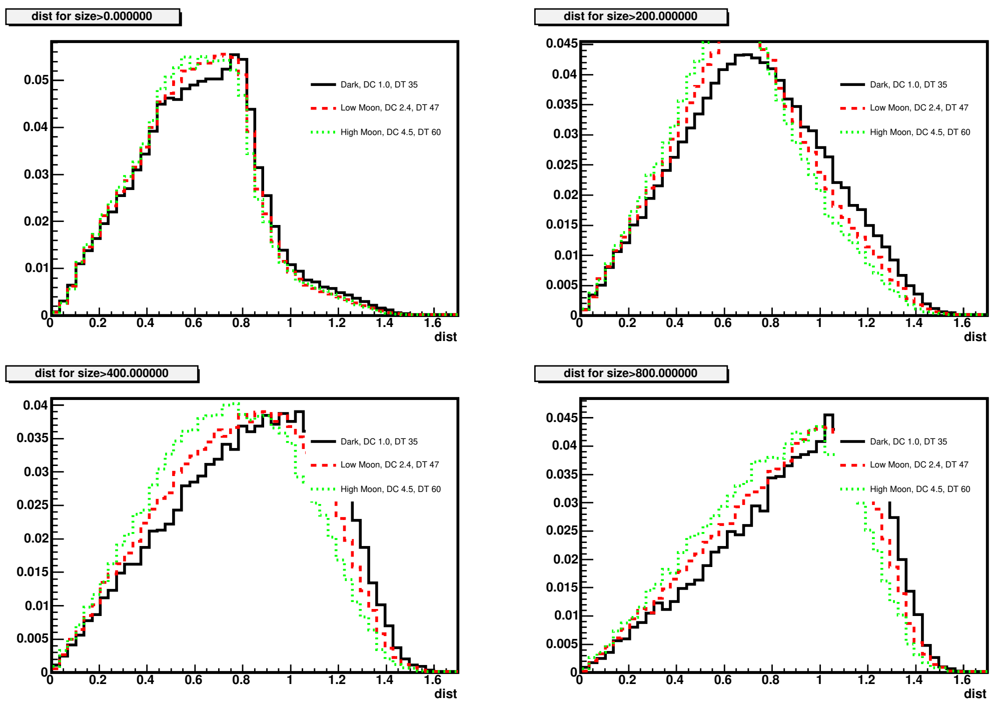

Figure 6: Distributions of DIST (in degrees) for three example Crab Nebula samples with different moonlight conditions and different SIZE lower cuts. The histograms are normalized to unit area.

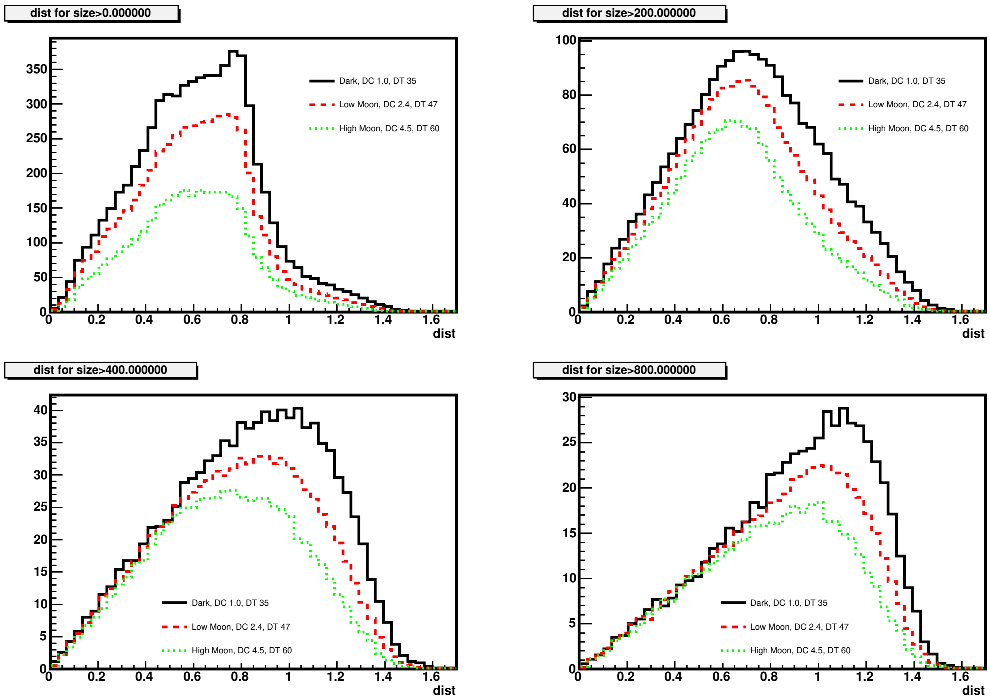

Figure 7: Distributions of DIST (in degrees) for three example Crab Nebula samples with different moonlight conditions and different SIZE lower cuts. The histograms are normalized to a common observation time.

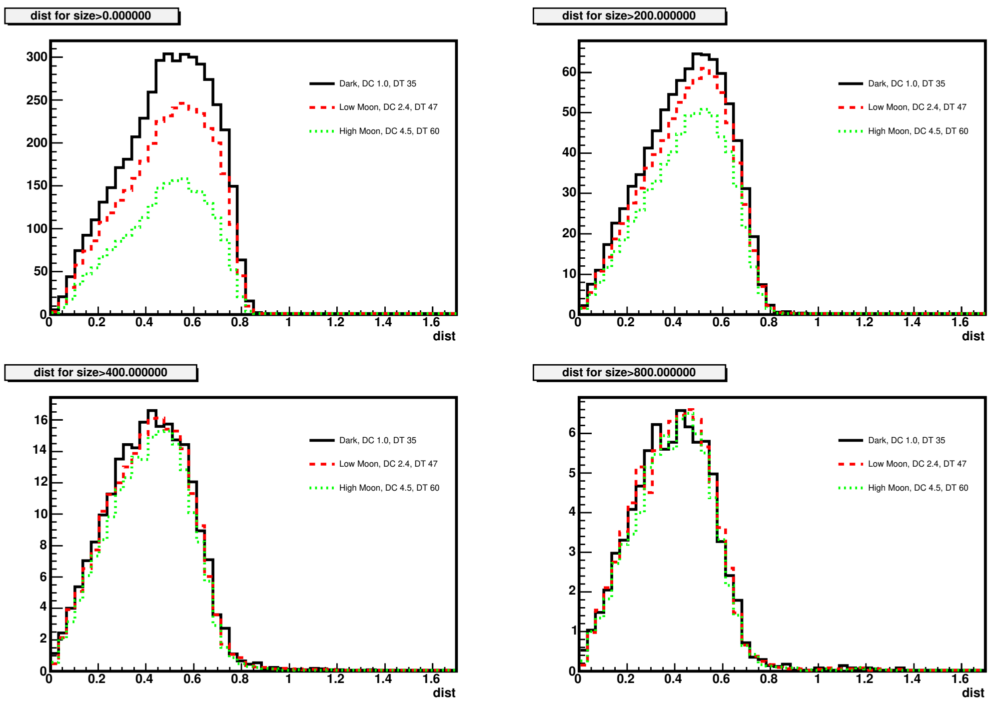

Figure 8: Distributions of DIST (in degrees) for showers fully contained in the inner camera, for three example Crab Nebula samples with different moonlight conditions and different SIZE lower cuts. The histograms are normalized to a common observation time.

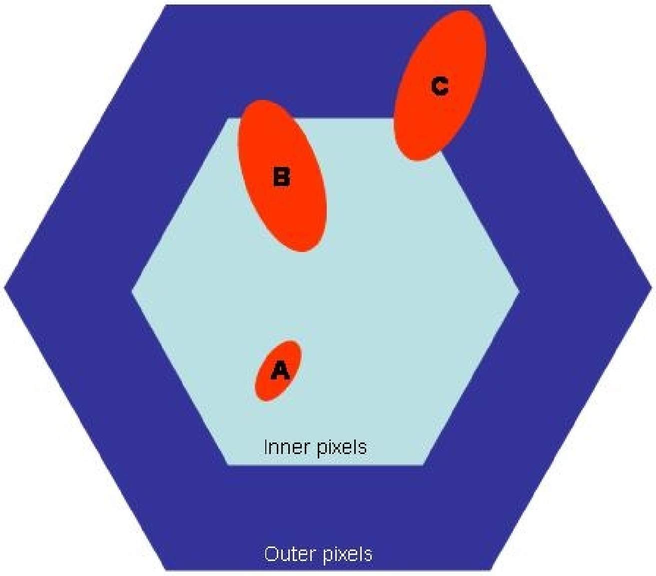

Figure 9: Schematic representation of the MAGIC camera with 3 showers of different SIZE. Marked with an A, a shower with a low SIZE may not fulfill the trigger conditions if discriminator thresholds are set to a high value. Showers that are fully contained in the trigger region (B) are well above the increased discriminator level, whereas showers of the same SIZE but a large DIST (C) are only partly contained in the trigger area and may not pass the higher DT

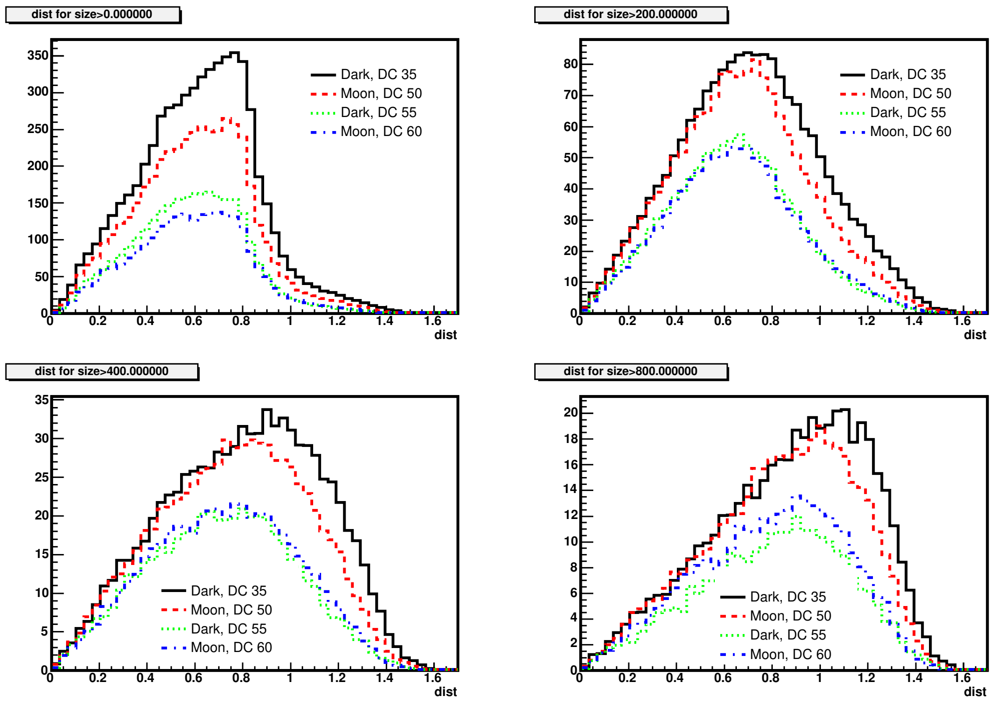

Figure 10: Distributions of DIST (in degrees) for three example Crab Nebula samples with different moonlight conditions plus a sample corresponding to dark observations with high DT values. The distributions are shown for different SIZE lower cuts and normalized to a common observation time.

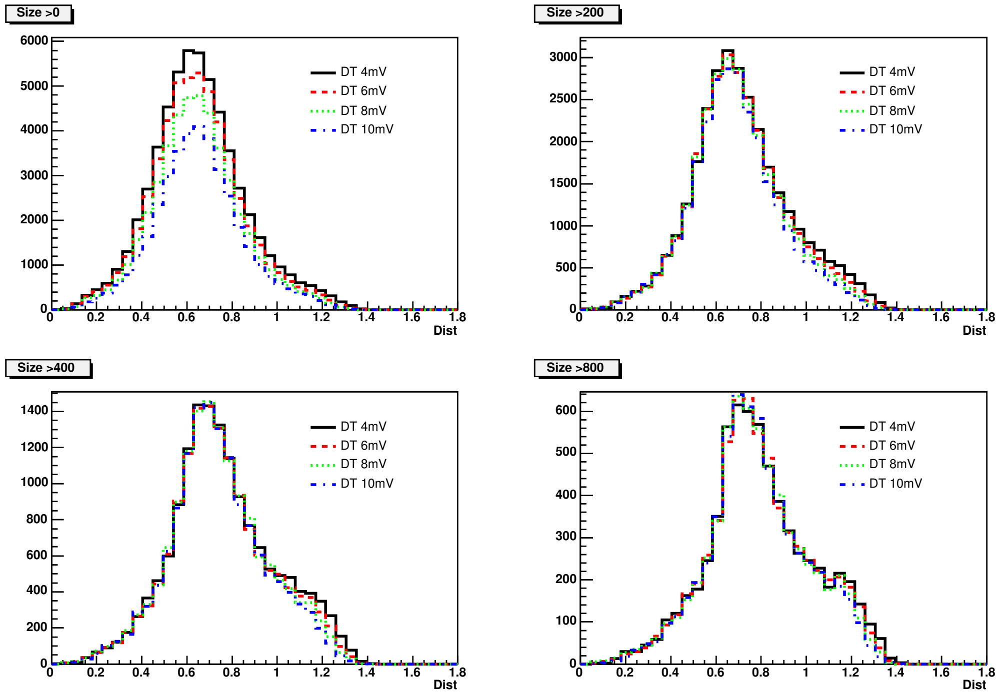

Figure 11: Distributions of DIST (in degrees) for MC simulated gamma-ray samples (see Table 2) considering different trigger threshold values and SIZE lower cuts.

image is collected by the outer pixels, and the fraction of the ellipse included in the trigger area may not be large enough to fulfill the trigger condition. This hypothesis was also confirmed by ways of a dedicated test. We observed Crab in dark conditions (DC$\sim$1.1 μA), but with the DTs set to 55. Unfortunately, the zenith angle of the test could not be matched to any of the samples analyzed here (see Table 1) but the agreement is good enough for our purposes. Figure 10 shows the DIST distribution for the test sample together with those for a DT selected according to the LONS level. It is evident that the distortion of the DIST distribution is not related with the mean DC current in the camera but only with the level of the discriminators.

4 Monte Carlo Simulations

We have compared the results presented in the previous section with MC simulations. In the MC standard production, the default value of the discriminator level voltage is 4 mV, tuned to reproduce the rates for dark observations. In addition, we have processed the standard sample using 1, 2 and 4 times the default LONS level and discriminator values of 6, 8 and 10 mV (set 1 in Table 2). Assuming a linear dependence of the DTs with the discriminator voltage, those would correspond to DT 53, 70 and 88 arbitrary units, respectively. The DIST distribution for the different DTs are compared in Figure 11. The loss of events observed in the data at all SIZE values is not reproduced in the MC. This means either that gamma-rays are actually less affected than hadrons due to their different DIST distributions, or that there is a problem with the simulation of the trigger in MC. On the other hand, no significant change was observed in the DIST distribution corresponding to the different LONS levels that could explain the difference in the Hillas distributions.

In order to discriminate between the two possibilities we performed the following test. From

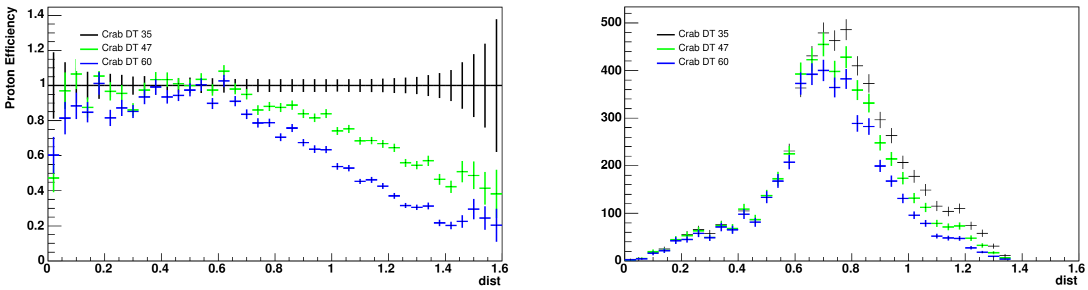

Figure 12: Left: selection efficiency curves as a function of DIST for DTs 35, 47 and 60, computed from data (see Figure 7). Right: convolution of the MC DIST distribution (DT_{MC} = 4 mV) with the efficiency curves obtained from data for DTs 35, 47 and 60. A cut SIZE > 400 phe has been applied.

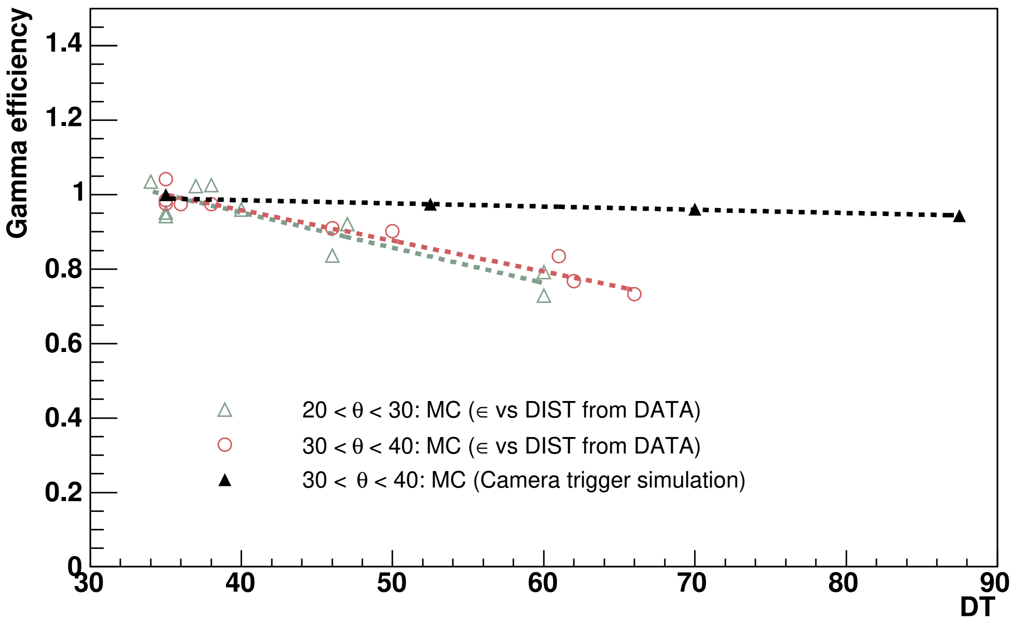

Figure 13: Monte Carlo gamma-ray selection efficiency (ϵ) as a function of the DT (with respect to DT=35) for SIZE>400 phe computed using the efficiency vs DIST obtained from data (open markers) and by the standard trigger simulation (solid markers). In the latter case a linear dependence between the trigger voltage and the DT value has been assumed. Also shown are the results of the linear fits (efficiency≡1 for DT=35) to the different considered samples.

real data we can compute, for a given DT, an event selection efficiency as a function of DIST, with respect to the standard (DT=35) case. As an example, we will show the results for a SIZE cut of 400 phe and DT values 35, 47 and 60. From Figure 7 (bottom-left panel) we can compute the efficiency curves as a function of DIST dividing, bin to bin, the histograms for DT 35, 47 and 60 by that for DT 35. The results are shown in Figure 12 (left panel). These efficiency curves can be convoluted with the DIST distribution for the MC standard sample (threshold 4 mV, sets 3 and 4 according to the data zenith angle). The results are shown in Figure 12 (right panel). This should correspond to the DIST distribution of MC samples simulated with threshold values 5.4 and 6.9 mV, respectively, under the following assumptions: first, we neglect any other factor which could affect the loss of events but the DT; second, we consider that, in first approximation, the increase of the DTs has the same effect on hadrons and gamma-ray events. The former assumption has already been validated with data (see Section 3), the latter one will be checked later by comparison of gamma-ray selection efficiency computed from data and from MC.

From the total number of events in the modified DIST distributions we can compute a global gamma selection efficiency with respect to the standard case (DT=35) for different DT values. We have done such a calculation using the efficiency curves as a function of DIST computed from all the Crab data samples (see Table 1). The gamma selection efficiency obtained by folding such curves with the MC standard production, for the two considered zenith angle bins and SIZE>400 phe, are shown in Figure 13. Also shown are the results obtained using the direct simulation of the trigger in the MC. The gamma-ray efficiencies obtained from these two approaches do not agree. This points to the possibility that the trigger simulation could be not properly implemented in the standard MC camera program. A comparison with gamma-ray efficiencies obtained from data (presented later), and the fact that this deficiency is suspected by the MC experts [9], also support this hypothesis.

5 Gamma-ray Efficiency and Sensitivity

The gamma-ray detection efficiency as a function of the DT can be computed from data using Crab Nebula observations. We have applied the analysis described in Section 2 to all Crab Nebula data samples listed in Table 1 (with further subdivision in DT bins when possible). For each of the samples we get a measure of the gamma-ray rate, i.e. the number of excess events per unit time. The dependence of the rate (R) with the DT is well fitted using a linear function:

$$R = A\,(1 - S_\epsilon\,(DT - DT_0)) \tag{1}$$

where A is a normalization factor (the rate for $DT = DT_0$), S_ϵ is the efficiency loss rate, and DT_0 is a reference DT value that, for convenience, is chosen as the one used in dark observations, i.e. $DT_0 = 35$. The value of A is irrelevant for this study and we present the results for $\epsilon \equiv R/A$, i.e. the gamma-ray efficiency with respect to the case $DT = DT_0 = 35$ (dark observations). The results for SIZE>400 and the two considered zenith angle bins ($[20°, 30°]$ and $[30°, 40°]$) are shown in Figure 14. The parameters of the fit obtained from both zenith angle domains are compatible within statistical errors. This allows us to perform a combined fit for all data samples. We obtain the following expression for the gamma-ray efficiency:

$$\epsilon = 1 - (1.41 \pm 0.32) \times 10^{-2}(DT - 35) \quad [\pm 0.1] \tag{2}$$

The first error quoted is the error on the slope as obtained from the fit and it does not include any correlation with the normalization factor. The second error quoted is an overall uncertainty obtained from the residuals of the individual data points to the fit (inset in Figure 14). This most likely comes from variations in the experimental conditions (weather, hardware, etc) between different observation nights. It is noteworthy that the linear function describes reasonably well the dependence of the efficiency with the DT, but day-to-day fluctuations of the order of 10% even for the case of dark observations are observed. This result is completely general, and can be regarded as a measure of the systematic point-to-point uncertainty when measuring light-curves. The gamma-ray efficiency is reduced by 1.41% per DT count, implying that, for strong illumination of the camera, efficiency losses up to 50% are expected. Moreover, this result seems

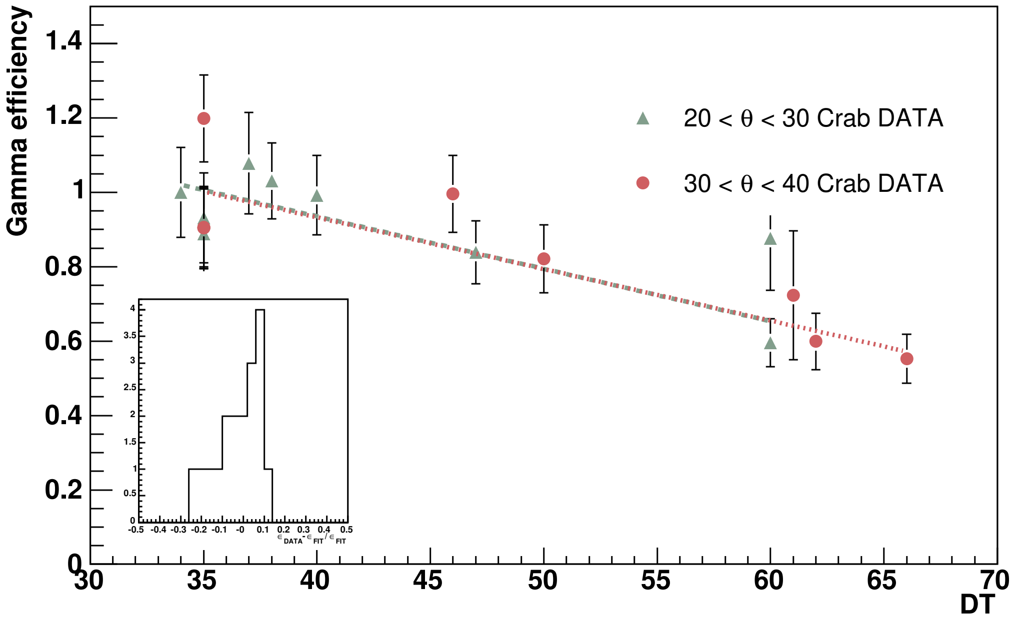

Figure 14: Gamma efficiency as a function of the DT for SIZE>400 phe and zenith angle bins $[20°, 30°]$ and $[30°, 40°]$ as measured using Crab Nebula observations. Also shown are the results of the fit of a linear function for both sets independently. The inset shows the residuals to the data points to a common linear fit.

to be independent of the zenith angle. A study of the dependence of S_ϵ with the SIZE cut will be presented in Section 6.

We compare these results with the ones obtained in the previous section for MC. In Figure 15 we show the results of the fit to the gamma-ray efficiency measured from Crab Nebula observations (from Figure 14), together with the values obtained for the MC folded with the efficiency as a function of DIST (from Figure 13). This comparison shows a discrepancy between data and MC. However the differences are even larger when we compare with the MC standard trigger simulation. This confirms that there is a problem in the simulation of the trigger in the standard camera program. However, the fact that there is a discrepancy between the results from data and MC tells us that our initial hypothesis, namely that the dependence of the efficiency with DIST is the same for gamma than for hadron events, is not fully correct. The result from MC convoluted with efficiency curves vs. DIST obtained from hadrons overestimate the gamma-ray detection efficiency. This means that the real efficiency curve for gamma events must be lower at least for DIST values between ∼0.5 to ∼0.8, where most of the gamma events concentrate. This is an expected effect, since gammas are pointing to the center of the camera, and therefore the probability of a high fraction of the shower to lie out of the trigger region is higher than for hadrons, that are randomly oriented. However, this does not necessarily mean that the overall loss of gammas is higher than that of hadrons, since the convolution of the efficiency curve with the DIST distribution (that peaks at higher values for hadrons) can still give higher overall losses of hadrons. As we will show next, this is actually the case.

We have also measured the loss of sensitivity produced by the increase of the DTs. In doing so we have used the standard sensitivity definition [10] and computed the loss with respect to

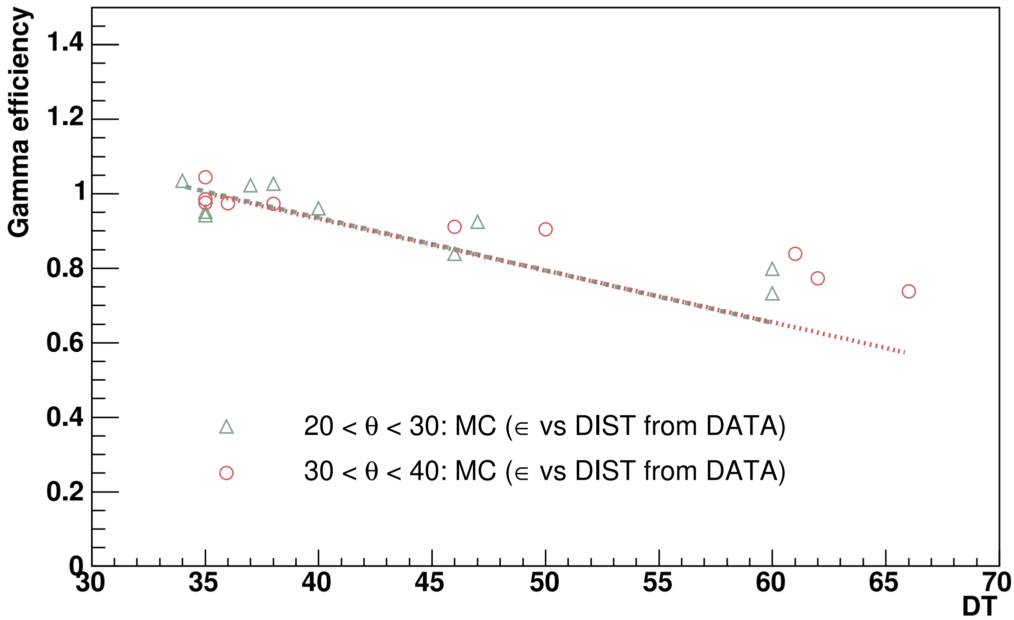

Figure 15: Comparison of the gamma-ray efficiency as a function of the DT for SIZE>400 phe as obtained from data (lines) and from MC convoluted with efficiency provided by the DIST distributions (dots) for zenith angle bins $[20°, 30°]$ and $[30°, 40°]$

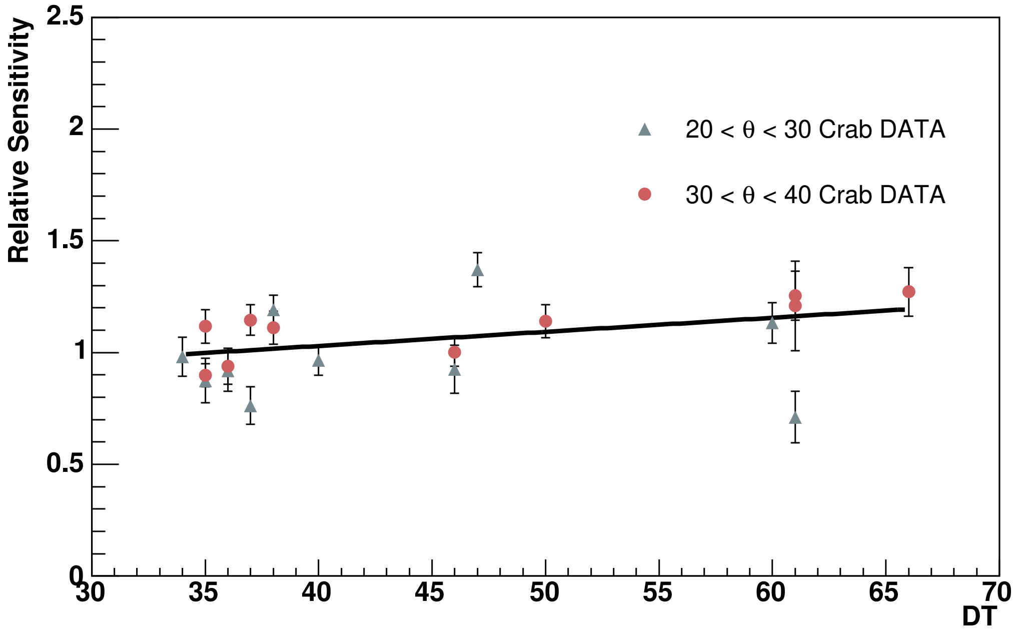

Figure 16: Relative sensitivity vs DT for a lower SIZE cut at 400 phe and zenith angle bins $[20°, 30°]$ and $[30°, 40°]$, measured from Crab Nebula observations. Also shown are the result of the fit of a linear function for both sets.

the sensitivity at DT=35 (s_0). The loss is defined by:

$$s/s_0 = \frac{N_\gamma^0 \sqrt{N_{\rm bkg}}}{N_\gamma \sqrt{N_{\rm bkg}^0}} \tag{3}$$

where N_γ and $N_{\rm bkg}$ are, respectively, the number of excess and background events in the signal region (see Section 2). The superindex 0 stands for the values for DT=35. The results for SIZE>400 phe and all Crab Nebula data samples are shown in Figure 16. The dependence of the sensitivity with DT is well fitted by the following linear function, parametrized again as $s/s_0 = 1 + S_s(DT - 35)$:

$$s/s_0 = 1 + (6.3 \pm 1.6) \times 10^{-3}(DT - 35) \tag{4}$$

Therefore, there is a loss of sensitivity of 6.3‰ per DT unit. This number is to be compared with the 1.4% loss in the gamma efficiency obtained in Equation 2. For instance at DT=60 we get a gamma-ray efficiency of 65% but the sensitivity worsen only by 15% (e.g. from a 2.5% to a 2.9% of the Crab Nebula flux), which is of the order of day-to-day fluctuations, as shown also in Figure 16. This means that the loss of hadrons is higher than that of gamma-rays, so that the sensitivity is not very much affected. Indeed, it can be computed from Equations 2 and 4, and confirmed with data, that the hadron efficiency falls with a rate of $\sim 1.6\%$ per DT count. This is not a surprising effect if we take into account that the loss of showers increases with DIST, and that hadrons peak at higher DIST values than gammas.

6 Dependence on SIZE/Energy

The results obtained in the previous section are valid for SIZE>400 phe. We have repeated the same study for four bins of SIZE, namely [200,400], [400,800], [800,1600] and [1600,6400] phe. The gamma-ray efficiencies as a function of the DT are shown in Figures 17 (for zenith angles between 20° and 30°) and 18 (for zenith angles between 30° and 40°). We find that in all cases Equation 1 describes reasonably well the data. The efficiency loss rate (S_ϵ) decreases as SIZE increases since the probability of passing a high trigger level is larger for larger images. For high enough values of SIZE the efficiency remains constant with DT.

The values of S_ϵ for the different size and zenith angle bins are listed in Table 4. We observe no significant discrepancies in the gamma-ray efficiency between medium and low zenith angle showers. In Figure 19, we represent S_ϵ as a function of SIZE. The position of the points along the x-axis is taken as the mean of the SIZE distribution for MC gamma-rays (standard simulation) after analysis cuts. We find a linear dependence that can be parametrized by:

$$S_\epsilon = -(2.24 \pm 0.13) + (7.2 \pm 1.2) \times 10^{-4} \text{ SIZE [phe]} \tag{5}$$

where the errors quoted are obtained from the fit, and include the correlation between the two free parameters. This is a very useful result since, together with Equation 1, allows to compute the gamma-ray efficiency loss for any SIZE and DT value (i.e. for all moonlight conditions). The result has been shown to be rather independent of the zenith angle, at least for values lower than 40°. An error in the efficiency of $\sim 10\%$ coming from day-to-day variations should be understood, as discussed in Section 5.

The same analysis is done to evaluate the sensitivity loss rate in SIZE bins. Figure 20 shows the relative sensitivity as a function of the DT for the 4 different SIZE bins. At lower SIZE values the relative sensitivity s/s_o degrades with increasing DT reaching a maximum value of

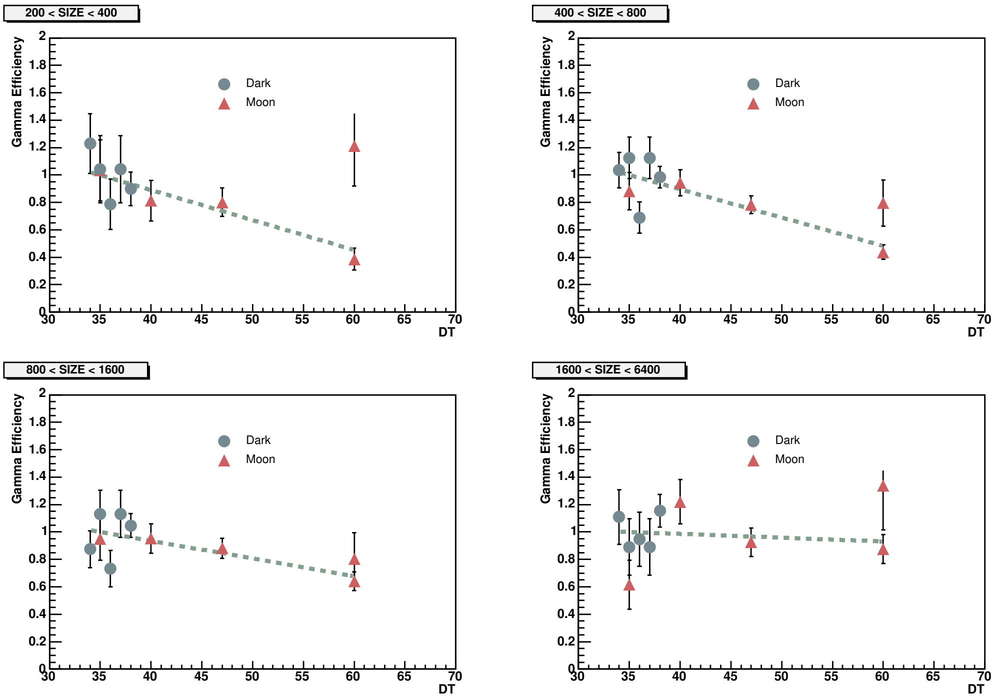

Figure 17: Gamma efficiency as a function of the DT for different SIZE bins and zenith angle bin $[20°, 30°]$, measured from Crab Nebula observations. Also shown are the result of the fits by a linear function.

Zenith Angle [deg]	SIZE [phe]	S_ϵ $[\times 10^{-2}]$	$\pm\ \Delta S_\epsilon$ $[\times 10^{-2}]$
$20-30$	200-400	2.2	0.3
	400-800	2.1	0.2
	800-1600	1.3	0.2
	1600-6400	0.3	0.4
$30-40$	200-400	2.0	0.2
	400-800	1.7	0.2
	800-1600	1.4	0.2
	1600-6400	0.4	0.4

Table 4: Gamma efficiency loss rate per unit DT obtained from Crab Nebula observations in different SIZE and zenith angle bins. The errors quoted are those obtained in the fit.

50%, while for higher SIZE values it remains constant with DT. The sensitivity loss rate as a function of SIZE is shown in Fig 21. A linear fit to the data yields:

$$S_s = (1.65 \pm 0.14) - (8.8 \pm 2.1) \times 10^{-4}\ \text{SIZE [phe]} \quad (6)$$

The results for the linear fits, merging the data from the 2 zenith angle bins, are quoted in Table 5.

We tested the dependences quoted in Eq. 6 and 5 under different HADRONNESS and ALPHA cuts, obtaining in all cases results compatible with statistical and systematic uncertainties.

Finally, it is important to understand the effect of the moonlight in the energy threshold. Using a MC sample we compute the energy threshold as the median of the energy distribution for

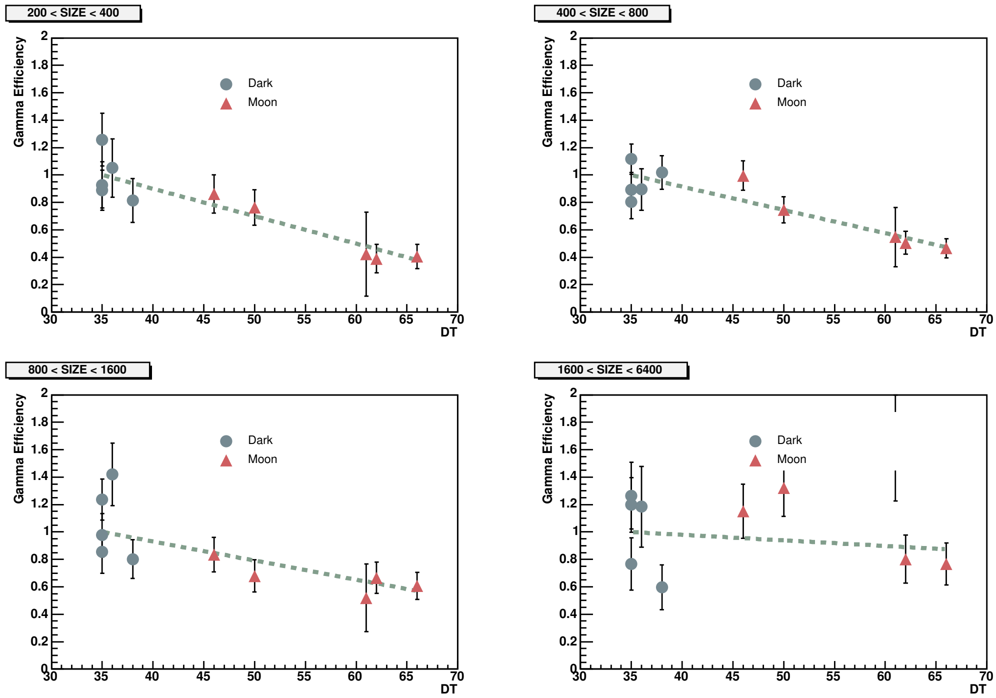

Figure 18: Gamma efficiency as a function of the DT for different SIZE bins and zenith angle bin $[30°, 40°]$, measured from Crab Nebula observations. Also shown are the result of the fits by a linear function.

gamma-ray events. Due to the problems of the trigger simulation in the standard MC program discussed in Section 4, we have to follow an approximation. We process MC set 3 (Table 2) with the camera program, with discriminator values $\mathrm{DT_{MC}} = 4$, 10, 30 and 50 mV. The gamma-ray efficiency vs $\mathrm{DT_{MC}}$ above 400 phe (see Figure 22) is compared to that obtained for data (see Figure 14), and a calibration factor from $\mathrm{DT_{MC}}$ to DT is obtained. We have checked that the results does not depend on the LONS level by repeating the analysis with a MC sample with increased LONS level (set 2). The efficiency as a function of $\mathrm{DT_{MC}}$ derived from Figure 22 can be expressed as:

$$\epsilon_{\mathrm{MC}} = 1 - (1.59 \pm 0.05) \times 10^{-2} (DT_{\mathrm{MC}} - 4) \tag{7}$$

and by comparison with equation 2, leads to:

$$DT_{\mathrm{MC}} = 0.88\ (DT - 35) + 4 \tag{8}$$

To test the consistency of MC and data, we calculate the efficency loss rate (S_{MC}) in bins of SIZE and use expression 8 to compare with the results obtained for Crab Nebula (see Table 6). The values of S obtained from data and MC, that is, S_ϵ and S_{MC}, are compatible within statistical errors. This check gives us confidence to extract the value of the threshold from the MC simulated samples. We have computed different levels of threshold, namely:

- Trigger energy threshold after calibration without applying any cleaning level (green stars in Figure 24). The peak energy for dark observations is 55 GeV.
- Energy threshold after two different cleaning levels, an absolute cleaning level of 10,5 represented with black squares in Figure 24, which is the one applied in La Palma standard

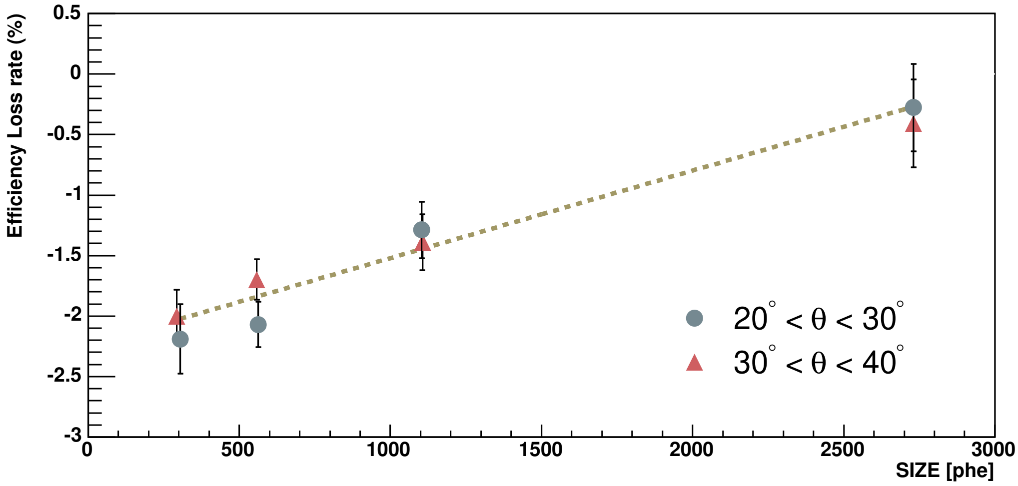

Figure 19: Gamma efficiency loss rate (S_ϵ) as a function of SIZE obtained from Crab Nebula observations at zenith angles between 20° and 40°. The line represents the result of a linear fit to the data points.

Zenith Angle [deg]	SIZE [phe]	S_s [$\times 10^{-2}$]	$\pm\ \Delta S_s$ [$\times 10^{-2}$]
$20 - 40$	200-400	1.4	0.1
	400-800	1.3	0.2
	800-1600	0.7	0.4
	1600-6400	-0.4	0.4

Table 5: Sensitivity loss rate per unit of DT obtained from Crab Nebula observations in different SIZE. The errors quoted are those obtained in the fit. The analysis is done considering the two zenith angle ranges together since no significant variation is seen between the 2 samples.

analysis, used in this paper. And a less restrictive absolute cleaning level of 7,5 in blue circles. The peak energy at the lower DT value are 84 and 66 GeV respectively.

- Finally we applied the same analysis used to extract gamma-ray from the Crab Nebula data and compute the so called analysis threshold (in red squares in the Figure).

The energy distributions before analysis cuts for 10,5 absolute cleaning level and for different DTs are shown in Figure 23. We fit a Gaussian function in a restricted region centered at the distribution's median, and extract the threshold as the value of Gaussian mean obtained in the fit. The same procedure is done for Monte Carlo events after analysis cuts and for different cleaning levels. The dependence of the analysis energy threshold for cleaning level 10,5 is well described by a linear function:

$$E_{\mathrm{th}} = 79 + 10\ (DT - 35) \qquad [\mathrm{GeV}] \tag{9}$$

The analysis threshold is obviously higher than the trigger threshold for normal (dark) observations due to the higher Q-factors for lower SIZE values. This difference vanishes for increasing DT since low SIZE showers do not trigger the camera. At the maximum moon illumination (for a mean DT of 60) the analysis energy threshold increases by a factor of 2.

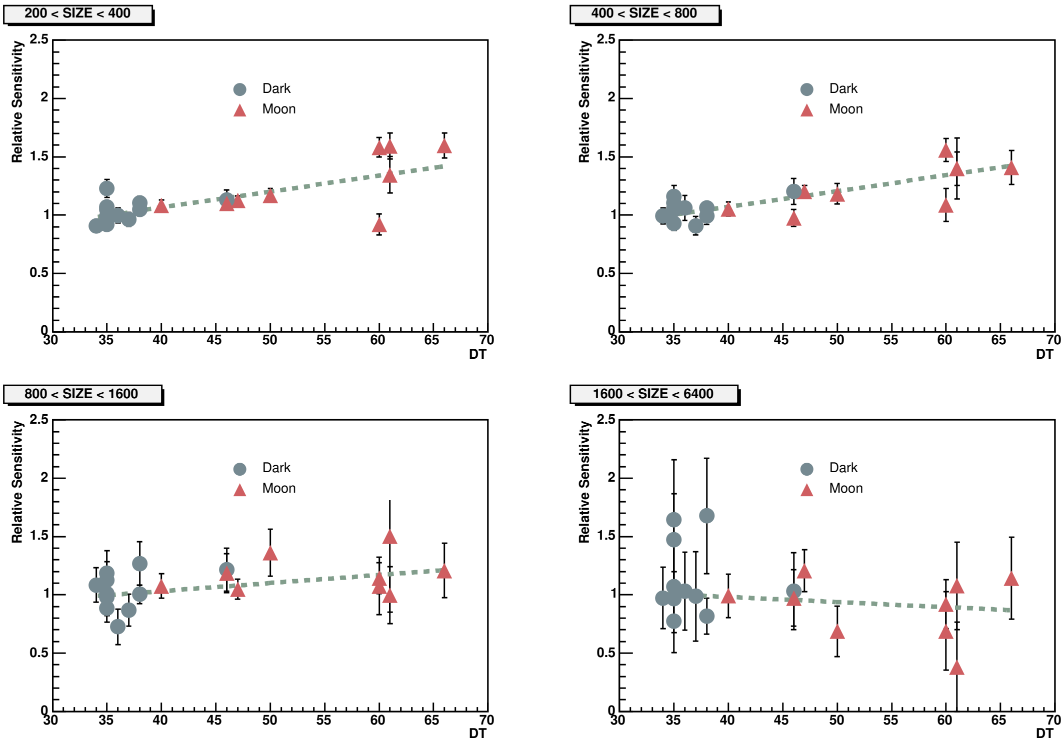

Figure 20: Relative sensitivity as a function of DT obtained from Crab Nebula data in different SIZE bins. Data from medium and high zenith angles are merged since no variation in the tendency was found. The line represents the result of a linear fit to the data points.

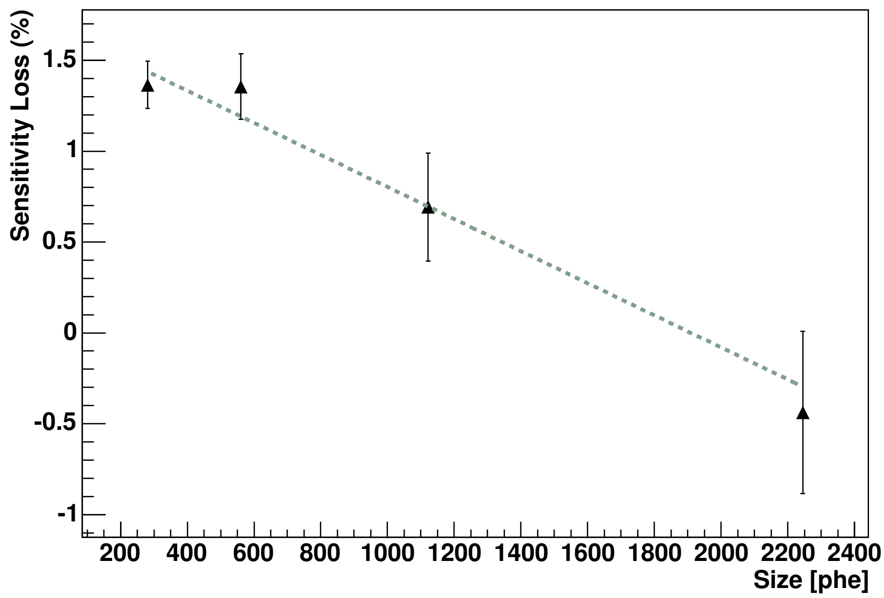

Figure 21: Sensitivity loss rate (S_s) as a function of SIZE obtained from Crab Nebula observations at zenith angle between 20° and 40°. The data are consistent with a linear fit.

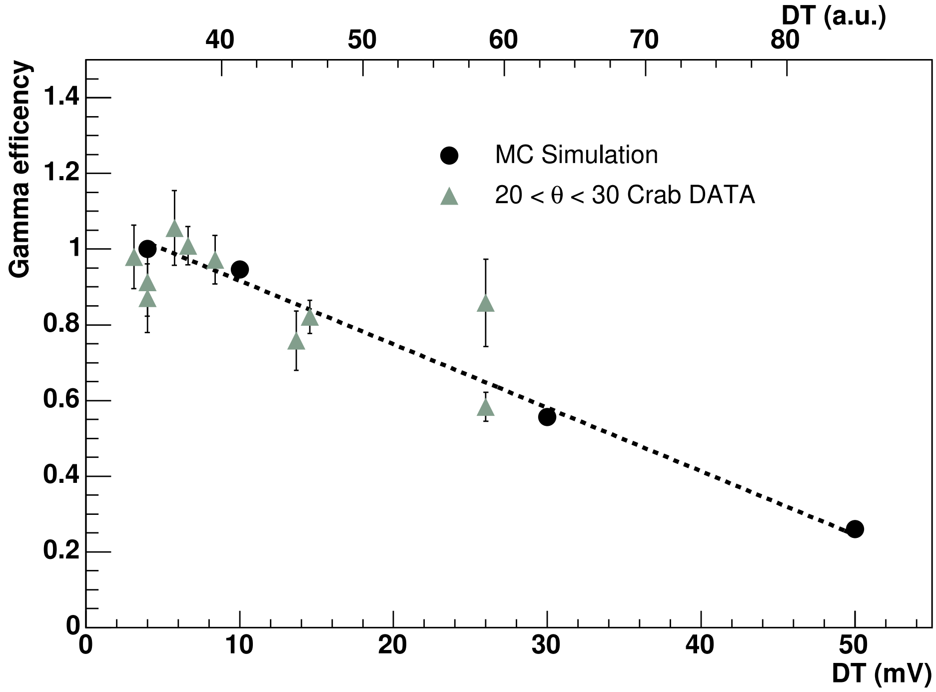

Figure 22: MC gamma-ray efficiency above 400 phe as a function of the DT_{MC} (in units of mV as included in the standard MC simulation program). For comparison, the top axis shows the value of DT and in green triangles Crab data gamma ray efficiency is superimposed to the MC data to show the agreement.

Zenith Angle [deg]	SIZE [phe]	S_ϵ [$\times 10^{-2}$]	$S_{\rm MC}$ [$\times 10^{-2}$]
$20 - 30$	200-400	2.2 ± 0.3	2.5 ± 0.2
	400-800	2.1 ± 0.3	2.1 ± 0.09
	800-1600	1.3 ± 0.2	1.0 ± 0.07
	1600-6400	0.4 ± 0.4	0.3 ± 0.08

Table 6: Comparison of the gamma-ray efficiency loss rate measured from data and MC for different SIZE bins.

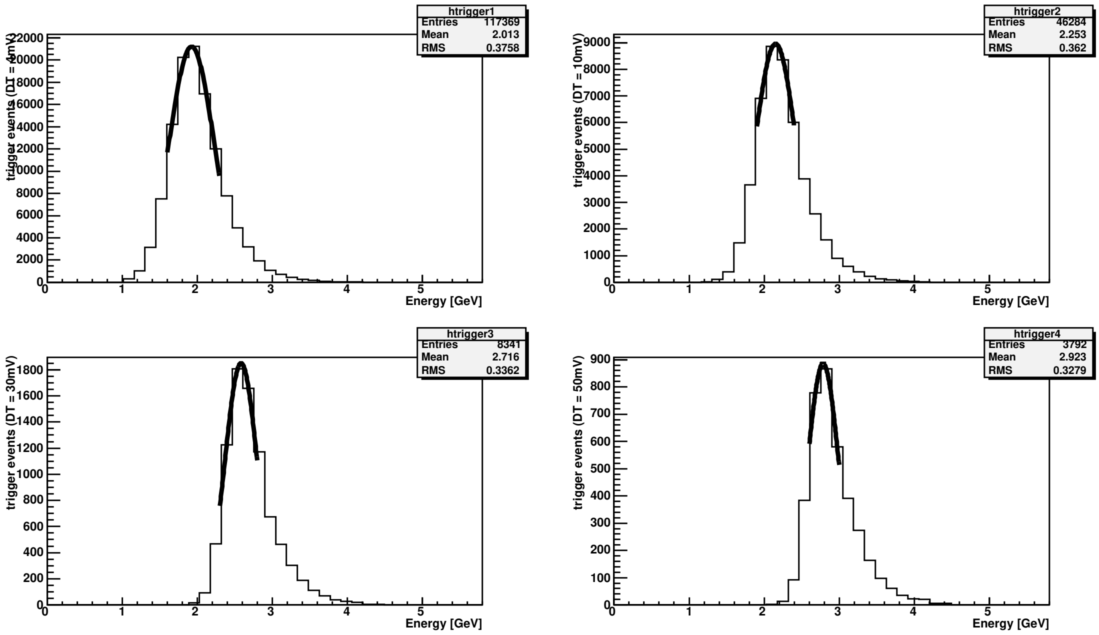

Figure 23: Energy distribution of MC gamma-ray events (cleaning 10,5) for different levels on the discriminator thresholds. The lines represent the results of a Gaussian fit to a restricted region centered at the distribution's median.

From the above expression, the energy threshold increases 10 GeV per DT unit. Both, the analysis and cleaning thresholds could decrease to lower energy values if a special treatment of the data (e.g., low zenith angle observations and timing cleaning) was applied, which is not the case in this work.

7 Conclusions

We have characterized the telescope's response in observations under moderate illumination, e.g. with moderate moonlight or twilight, using Crab Nebula observations and Monte Carlo simulated gamma-ray events. We have used data in two zenith angle bins, namely $[20°, 30°]$ and $[30°, 40°]$, obtaining compatible results in all cases. The dominant effect is given by the fact that the discriminator thresholds have to be increased in order to keep the rate of accidentals reasonably low. The LONS level itself has been shown to contribute in a comparatively negligible way. The Hillas distributions, and in particular the HADRONNESS distribution, are not very much distorted, and the gamma/hadron separation power is not severely affected. One important consequence is that the analysis of moonlight and twilight data needs no special treatment, at least in what regards the calibration, the image cleaning and the gamma/hadron separation.

All our results can be parametrized as a function of the mean DT. It is important that, during MAGIC operation, the DTs are set to a minimum value ensuring both, a low rate of accidental trigger events, and a minimal gamma-ray efficiency loss. Although we have not performed any study about the effect of the DT dispersion on our results, one would expect that a narrower DT distribution would lead to more stable results, whereas a wider one could be a source of camera inhomogeneities and instabilities. It is therefore important that the DT are increased or lowered according to the LONS level in a coherent way.

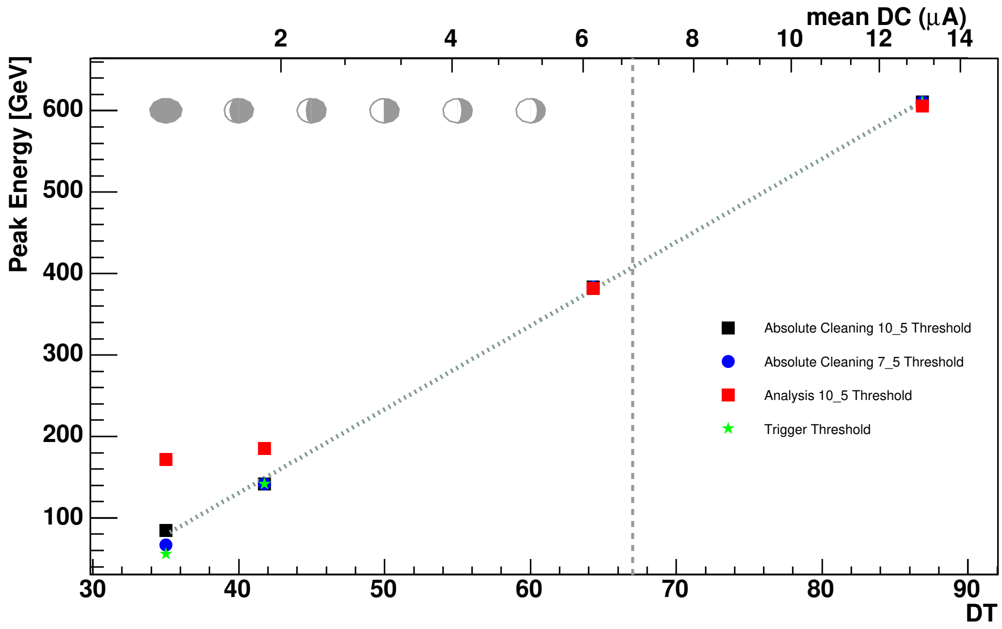

Figure 24: Trigger, cleaning and analysis energy thresholds as a function of the DT obtained from MC simulated gamma-ray events. The top axis shows the typical mean DC for a chosen DT value. The vertical line marks the maximum mean DC allowed for a safe operation of the MAGIC camera.

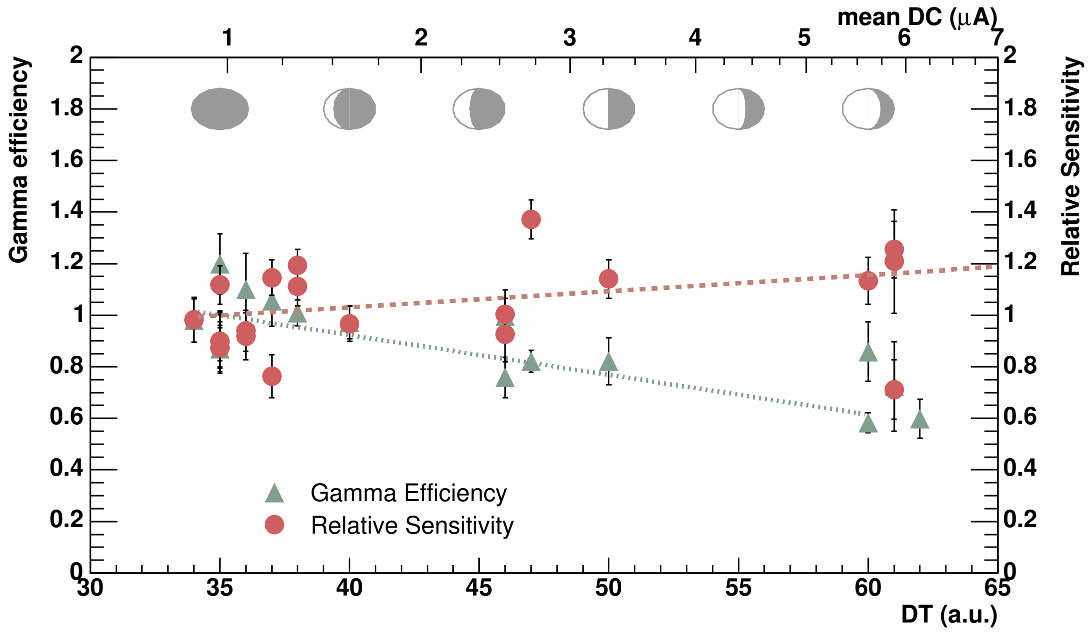

Figure 25: Effect of the moon observation for gamma efficiency (green dotted line) and sensitivity (red dashed line) for increasing DT (SIZE $>$ 400 phe). The top axis shows the mean DC values, from which different DT values are assigned and a schematic view of the moon light, although the mean DC value does not only depend on the moon phase but also on the angular distance to the camera/telescope.

We have compared our results to those obtained with gamma-ray samples simulated using the standard MAGIC MC camera program. We have found a deficiency in the simulation of the trigger. This probably does not affect analyses carried out so far, since the analysis threshold is still well above the trigger threshold, but it is important to this study. In order to determine the trigger dependence with the mean DT, we have performed a simple calibration of the MC trigger level and obtained an (expected) linear dependence of the trigger threshold with the mean DT. The (standard) analysis threshold increases by a factor 2 for strong camera illumination.

We have found important effects in terms of losses in the gamma-ray detection efficiency at all energy/SIZE values. The sensitivity is not very much affected, due to the fact that hadrons also suffer from detection efficiency losses which, due to their higher mean DIST value, happen to be slightly higher (Fig.25) than those for gamma-rays. Actually, the loss of sensitivity that we measure is compatible with zero at SIZE high enough, while for small images the effect becomes important. Regarding the degradation of the gamma-ray efficiency, we have found a linear dependence with the DT mean value for all SIZE domains. We have defined the gamma-ray efficiency loss rate (S_ϵ) as the slope of the linear fit to the gamma-ray efficiency vs DT mean value, and found a law to determine S_ϵ for any SIZE value. When analyzing moonlight or twilight data, the only concern, apart from the increase of the threshold, is to correct the number of gamma-ray events in a spectrum or light curve bin, by the efficiency corresponding to the given DT and SIZE values.

References

[1] D. Kranich et al, Astrop. Phys. **12** (1999) 65.

[2] E. Pare et al., Proc. of the 22nd International Cosmic Ray Conference Vol 1, Dublin (1991) 492.

[3] S.M. Bradbury *et al.* Proc. of Towards a Network of Atmospheric Cherenkov Detectors IV, Padova, Italy (1996) 182.

[4] A. Armada *et al.*, “Telescope Performance”, MAGIC TDAS 06-04.
A. Armada, “Characterization and some applications of the anode current monitoring system of the MAGIC telescope”. Master thesis, 2005.
Available at: http://wwwmagic.mppmu.mpg.de/publications/theses/

[5] Available at http://cvs.ifae.es/

[6] H. Bartko *et al.* “Comparison of Signal Reconstruction Algorithms for the MAGIC Telescope”, MAGIC-TDAS 05-03.
H. Bartko *et al.* Proc. of Towards a Network of Atmospheric Cherenkov Detectors VII, Palaiseau, France (2005) 555.

[7] M. Gaug *et al.* Proc. of the 29th International Cosmic Ray Conference Vol 5, Pune, India (2005) 375.

[8] P.Majumdar *et al.* Proc. of the 29th International Cosmic Ray Conference Vol 5, Pune, India (2005) 203.

[9] A. Moralejo and C. Bigongiari, private communitacion.

[10] A. Moralejo, “Monte Carlo estimate of flux sensitivity of MAGIC for point-like sources”, MAGIC-TDAS 04-04.